Mass number scaling in ultra-relativistic nuclear collisions from a hydrodynamical approach

J. Sollfrank[1,a], P. Huovinen[2], P.V. Ruuskanen[2]

[1] Fakultät für Physik, Universität Bielefeld, Germany
[2] Department of Physics, University of Jyväskylä, Finland

Abstract. We study the different nucleus-nucleus collisions, O+Au, S+S, S+Ag, S+Au and Pb+Pb, at the CERN-SPS energy in a one-fluid hydrodynamical approach using a parametrization based on baryon stopping in terms of the thickness of colliding nuclei. Good agreement with measured particle spectra is achieved. We deduce the mass number scaling behaviour of the initial energy density. We find that the equilibration time is nearly independent of the size of the colliding nuclei.

1 Introduction

From heavy ion collisions at ultra-relativistic energies one would like to learn, e.g. how high energy and baryon number densities can be reached in these collisions and to what degree the produced matter is equilibrated. Answers to these questions would tell us which regions in the nuclear phase diagram are accessible in nuclear collisions. It would also show if, and to what extent the quark-gluon phase has been reached in present SPS experiments [1].

There are no direct measurements of the achieved energy and baryon number densities and therefore one uses models to extract the information from the experimental data. One commonly used approach is hydrodynamics [2] which correlates the initial densities with measured spectra of final particles. By definition, hydrodynamics assumes local thermal equilibrium in the expanding matter and is therefore unable to answer the question of thermal equilibration.

Our main goal in this work is to investigate the scaling of initial energy density in heavy ion collisions as a function of the size of the colliding nuclei at (nearly) fixed energy. Therefore we study and compare five different collisions at CERN-SPS energies, O+Au, S+S, S+Ag, S+Au and Pb+Pb, using the same parametrization for the initial state. In Sect. 2 we introduce the parametrization of the initial conditions. Section 3 discusses the results and in Sect. 4 conclusions are drawn.

2 Initial conditions

At ultra-relativistic energies nucleus–nucleus collisions are expected to become transparent, meaning that the matter

ᵃ *Present address:* Institut für theoretische Physik, Universität Regensburg, D-93040 Regensburg, Germany
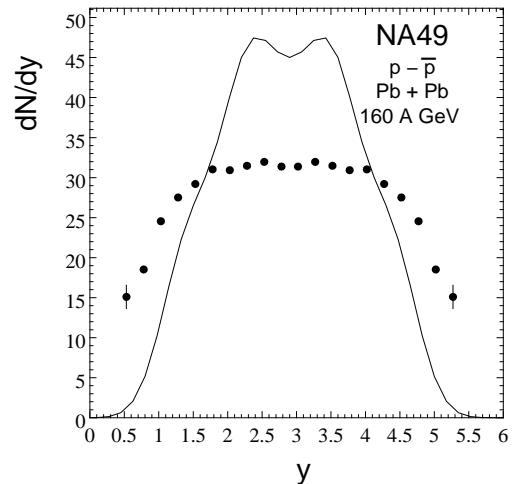
Fig. 1. Rapidity spectra of $p - \bar{p}$ in Pb+Pb collisions for the Landau initial conditions with no initial flow velocity. The calculated spectrum is compared with preliminary data from NA49 [3]

of final particles is produced in a state of *initial collective motion*. We have not succeeded to reproduce, even qualitatively, the baryon rapidity distributions if we assume that the produced matter is initially completely stopped, commonly referred to as the Landau initial conditions. As an example we show in Fig. 1 the net-proton distribution in a lead-on-lead collision as obtained by assuming that the matter of the initial fireball is at rest. The calculation is compared with the measurement of NA49 [3]. The disagreement between the data and the calculation is, as expected, larger for lighter nuclei. This indicates that the primary collision stage cannot be treated within one fluid hydrodynamics since this would lead to compressed matter at rest. Instead, we start the simulation after the

system has equilibrated [4,5]. To use this procedure we need a parametrization of the initial conditions. Little is known about the initial state and a chosen parametrization can be justified only by comparing with the data. The parameter space of the initial conditions, which give reasonable agreement with data turns out to be large. Partly this results from the freedom in choosing the equation of state. Therefore it is difficult to pin down, e.g. the initial temperature achieved in a heavy ion collision.

Here we exploit the idea to fix the initial conditions using the local thickness of colliding nuclei. We parametrize the nuclear stopping locally in the transverse direction in terms of the nuclear thickness function and then constrain the energy density from conservation of energy. The advantage of this approach, when combined with the geometry of the colliding nuclei, is that fixing of the parameters fixes the initial conditions for all different collisions at the given energy. It also gives a better basis to compare different collisions and to draw conclusions on the dependence of the initial state on the nuclear size.

The main features of our parametrization of the initial conditions are described in [6]. Here we summarize the most important ingredients. Note that we consider only impact parameter zero collisions i.e. azimuthal symmetry is assumed.

One of the difficulties in hydrodynamic simulations is the treatment of the surfaces. E.g. in the transverse direction the outer edges never behave hydrodynamically and even in head-on collisions a certain fraction of nucleons never suffer a single collision. These nucleons are not detected in the experiment and their energy does not contribute to the production of final matter. To account for this we use effective nuclear sizes, i.e. we replace the mass numbers of incoming nuclei, A and B by

$$A^{\text{eff}} = \xi A \quad , \quad B^{\text{eff}} = \xi B \qquad (1)$$

and fix the geometry in terms of these effective mass numbers A^{eff} and B^{eff}. In fixing the value of ξ, always close to one, we also compensate for the few percent losses of baryon number and energy in our numerical code.

We start out by parametrizing the rapidity distribution of baryons dN_{B}/dy as a sum of projectile and target contribution for symmetric collisions [6],

$$\begin{aligned}
\frac{dN_{\text{B}}}{dy} &= \frac{dN_{\text{B}}^{\text{P}}}{dy}(x_y) + \frac{dN_{\text{B}}^{\text{T}}}{dy}(x_y) \\
&= \left[C^{\text{P}} \exp(ax_y^3 + bx_y^2 + cx_y) \right. \\
&\quad \left. + C^{\text{T}} \exp(-ax_y^3 + bx_y^2 - cx_y) \right] (1 - x_y^2) , \quad (2)
\end{aligned}$$

using a variable $x_y = y/y_{\max}$, the rapidity scaled with $y_{\max} = y_{\text{cm}}^{\text{P}}$, the projectile rapidity in the cm frame. The factor $(1 - x_y^2)$ ensures that the distribution goes to zero at the boundary of the phase space when effects like Fermi motion are neglected. The functional form is motivated by the experimental proton rapidity distributions in $p + p$ collisions [6] and the possibility to control the amount of stopping. C^{P} and C^{T} are normalization constants. The main idea of our parametrization is that the above initial

distribution is determined locally in transverse plane. This is implemented by defining the parameters $a(T_A)$, $b(T_A)$ and $c(T_A)$ as functions of the local nuclear thickness

$$T_A(\rho) = \int dz \, n_{\text{B}}(z, \rho) , \qquad (3)$$

where $n_{\text{B}}(\mathbf{r})$ is the nuclear density for a nucleus of mass number A, z is the longitudinal and ρ the transverse variable: $\mathbf{r} = (z, \rho)$. We use the Woods-Saxon parametrization for the nuclear density

$$n_{\text{B}}(\mathbf{r}) = \frac{n_0}{\exp[(|\mathbf{r}| - R_A)/a_R] + 1} , \qquad (4)$$

with

$$R_A = 1.12 \, \text{fm} \times A^{1/3} - 0.86 \, \text{fm} \times A^{-1/3} , \qquad (5)$$

$a_R = 0.54$ fm and $n_0 = 0.17$ fm^{-3} [7]. The functional dependence of a, b and c on T_A is chosen to be [6]

$$\begin{aligned}
a(T_A) &= 1.5 \, (\sigma_{pp} T_A)^{-1} \\
b(T_A) &= \beta_s \, (1 - \sigma_{pp} T_A) \\
c(T_A) &= 3.0 ,
\end{aligned} \qquad (6)$$

where $\sigma_{pp} = 32$ mb is the total inelastic cross section for $p + p$ collisions at SPS energy. The first motivation for this parametrization is its simplicity. Second, in the case of one collision, i.e. $\sigma_{pp} T_A = 1$, the experimental proton rapidity distribution for $p+p$ collisions is recovered [6]. For $\sigma_{pp} T_A > 1$, the b coefficient is negative indicating increasing stopping with growing nuclear thickness, the strength being controlled by β_s. It is fixed from fits to baryon rapidity spectra in heavy ion collisions and therefore its determination includes the hydrodynamical evolution. Changing the hydrodynamical evolution by choosing different initial energy and (longitudinal) velocity distributions or equation of state results in different optimal values for β_s. In the analysis presented here the value $\beta_s = 2.25$ adequately reproduces all results.

For the initial local energy distribution we choose a Gaussian form

$$\frac{dE(\rho)}{dy} = C_\varepsilon \exp\left[\frac{-(y - y_0)^2}{2\sigma_\varepsilon^2} \right] \left[1 - (y/y_{\max})^2 \right] , \quad (7)$$

where the width σ_ε and the normalization C_ε depend on the transverse coordinate ρ. The normalization C_ε is given by energy conservation and the value y_0 is identified with the center-of-mass rapidity of the collision locally in the transverse plane. Since our hydrodynamic calculation is performed in the overall center-of-mass frame of participating nucleons, $y_0(\rho) \equiv 0$ for zero impact parameter collisions of equal nuclei. For asymmetric collisions the thickness of target and projectile varies differently with transverse radius ρ and therefore the rapidity of the local cm frame $y_0(\rho)$ changes in the transverse plane.

In (7) the only free parameter is the width σ_ε which is taken to depend on the nuclear thicknesses as [6]

$$\sigma_\varepsilon(\rho) = \frac{c_\varepsilon}{[\sigma_{pp} T_A(\rho) \sigma_{pp} T_B(\rho)]^{\alpha_\varepsilon}} , \qquad (8)$$

where σ_{pp} is included to make the denominator dimensionless. The constants c_ε and α_ε are determined from an overall fit to the investigated collision systems with the result $c_\varepsilon = 0.8$, $\alpha_\varepsilon = 0.125$ [1].

So far baryon density and energy density distributions are specified only as functions of velocities. To convert them into spatial distributions we have to specify the velocity field. In the case of the Bjorken model [8], the scaling ansatz for the longitudinal velocity is $v_z = z/t$ and initial conditions are usually defined at fixed proper time τ_0. Since scaling cannot hold in a finite system, we have, for numerical convenience, chosen the rapidity y instead of velocity v_z to have the linear z–dependence:

$$y(\rho, z) = \kappa(\rho)z, \qquad v_z(\rho, z) = \tanh[\kappa(\rho)z], \qquad (9)$$

where the proportionality constant κ depends on the transverse radius ρ [6]. For small z this ansatz can approach the velocity profile of the scaling solution. The proportionality constant is now κ instead of $1/\tau_0$ of the Bjorken model. We define

$$\tau_0^{\mathrm{eff}} = \frac{1}{\kappa(\rho = 0)} \qquad (10)$$

as a parameter which can be regarded as an equilibration time scale in the same way as τ_0 in the scaling case. The initial time τ_0^{eff} is a parameter which is expected to depend on the nuclear size and the collision energy and is adjusted separately to each collision.

As described above, the model is formulated for symmetric collisions in the center-of-mass frame of the collision. Since we are interested in the mass number dependence of the initial state and large part of the available data is for asymmetric collisions, we would like to modify the parametrization (2) to apply to arbitrary collisions, too.

In symmetric zero impact parameter collisions the rapidity shift is the same on the target and the projectile side and $y_0(\rho) = 0$ for all values of ρ. For asymmetric collisions the target and the projectile rapidities differ in the overall cm frame of the participating nucleons. Also, since we determine the initial conditions from the nuclear thicknesses locally in the transverse plane, we have to distinguish between the global cm frame and the cm frame for the collision of a row of target nucleons with a row of projectile nucleons at given ρ. Equation (2) is evaluated in this local cm frame with x_y defined using $y_{\mathrm{cm}}^{\mathrm{P}}$ on the projectile side and $y_{\mathrm{cm}}^{\mathrm{T}}$ on the target side

$$\begin{aligned}\frac{dN_{\mathrm{B}}}{dy}(y) &= \frac{dN_{\mathrm{B}}^{\mathrm{P}}}{dy}(y) + \frac{dN_{\mathrm{B}}^{\mathrm{T}}}{dy}(y) \\ &= \bigl[C^{\mathrm{P}} \exp(a_{\mathrm{T}} x_{y,\mathrm{P}}^3 + b_{\mathrm{T}} x_{y,\mathrm{P}}^2 + c_{\mathrm{T}} x_{y,\mathrm{P}}) \\ &\quad + C^{\mathrm{T}} \exp(-a_{\mathrm{P}} x_{y,\mathrm{T}}^3 + b_{\mathrm{P}} x_{y,\mathrm{T}}^2 - c_{\mathrm{P}} x_{y,\mathrm{T}})\bigr] \\ &\quad \times (1 + x_{y,\mathrm{T}})(1 - x_{y,\mathrm{P}}) , \end{aligned} \qquad (11)$$

where $x_{y,\mathrm{T(P)}} = y/|y_{\mathrm{cm}}^{\mathrm{T(P)}}|$ on the target (projectile) side. This ensures the important limit that for $T_{A,B} \to \infty$ the

<hr/>

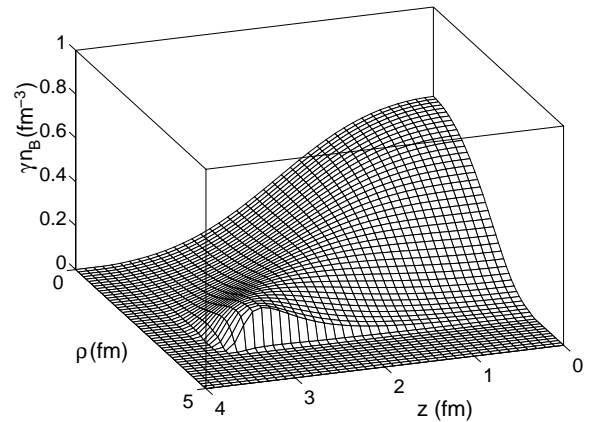[1] These values are slightly different from those used before in [6] due to the extension to more collision systems

Fig. 2. Initial baryon density distribution γn_{B} in the z-ρ plane for a S+S collision plotted in the overall center-of-mass frame at fixed initial time

system is stopped in the cm frame when we use (11) together with (6). Note that the distinction of local and global cm frames is necessary also if the parametrization is used for nonzero impact parameter collisions of equal nuclei.

We also have to modify the stopping parametrization to account for the fact that the rapidity of the local cm frame is shifted closer to the rapidity of the heavier nucleus. Without the modification this shift leads to too strong a stopping for lighter nucleus and too weak a stopping for the heavier one. Then the momenta of target and projectile nucleons after the collision will not add up to zero in the overall momentum frame. In principle this needs not to be the case since the mesonic degrees of freedom can balance the momentum but we do not find it plausible that the center of mass of nucleons would appreciable differ from the center of mass of produced mesons.

It turns out that the momentum balance between the colliding nucleons can be approximately satisfied if we replace T_A and T_B in (6) with effective values T_A^{eff} and T_B^{eff} defined as

$$\begin{aligned} T_A^{\mathrm{eff}} &= T_A \left(\frac{T_B}{T_A}\right)^\alpha \\ T_B^{\mathrm{eff}} &= T_B \left(\frac{T_A}{T_B}\right)^\alpha . \end{aligned} \qquad (12)$$

E.g., in the case $T_B < T_A$ we have $T_A^{\mathrm{eff}} < T_A$ which reduces the stopping of the lighter side in the parametrization (6) balancing the extra stopping from the shift of the local cm frame. At the same time the stopping of the heavier side is increased. The choice of $\alpha = 0.8$ leads to very satisfactory momentum balance within few percent for all three investigated asymmetric systems.

We conclude this section by depicting some examples of resulting initial density distributions. Since $T_A(\rho)$ depends on the transverse coordinate ρ the resulting stopping at the center is different from stopping at the edge. As an example we plot in Fig. 2 the baryon density γn_{B} in the cm frame for S+S collision. One sees clearly the increase in transparency with radius. This makes the one-fluid hy-
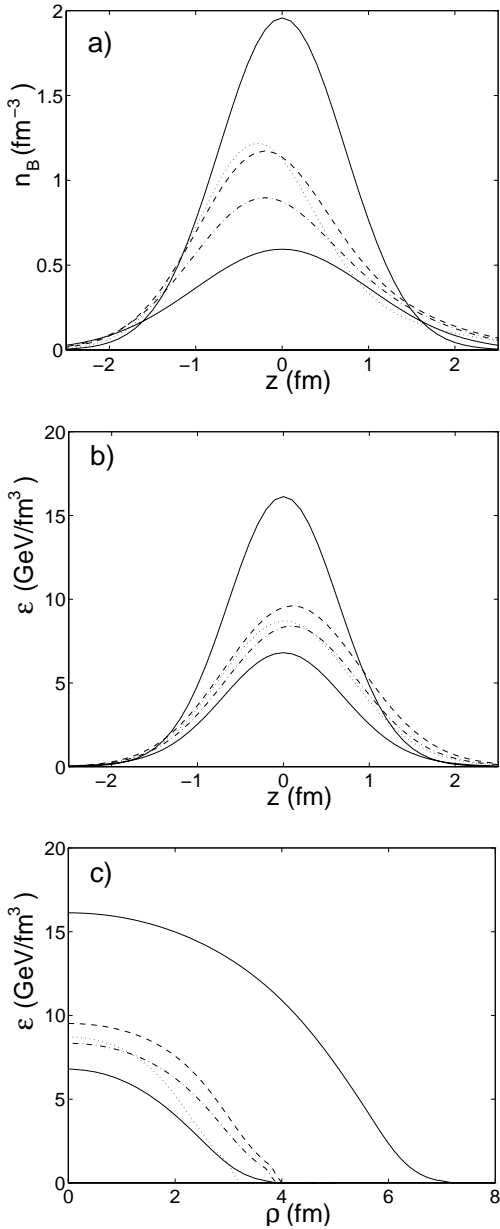
Fig. 4. Freeze-out contours $\varepsilon_f = 0.15$ GeV/fm^3 for the various collisions. The lines are as in Fig. 3

Figure 3b shows the local energy density $\varepsilon(z)$ for $\rho = 0$. It has a Gaussian form resulting from (7) and the linear fluid rapidity profile (9). For asymmetric collisions the maximum is at the local $y_0(\rho = 0) > y_{cm}^{AB} = 0$. In transverse direction the energy density is proportional to $T_A(\rho) T_B(\rho)$ resulting in the shapes shown in Fig. 3c.

3 Results

The above-described initial state is evolved in time by solving the ideal fluid hydrodynamical equations numerically on a 2+1 dimensional grid described in detail in [4] where different equations of state are compared. Here we show results only for an equation of state with phase transition to QGP at $T_c = 165$ MeV labeled as EOS A in [4].

Freeze-out occurs when the mean free path of particles is of the same order than the size of the fireball. For the collisions of light nuclei this criterium leads to freeze-out temperatures of $T_f \approx 140$ MeV [9]. Instead of taking contours of constant temperature we define the freeze-out on a space-time surface of constant energy density of $\varepsilon_f = 0.15$ GeV/fm^3. This results in an average freeze-out temperature of $T_f \approx 140$ MeV. The freeze-out contours are plotted in Fig. 4 for the different collisions we have studied. An increase in the size of the system leads to longer lifetimes as expected. One sees further that in asymmetric collisions the heavier target side lives longer.

For Pb+Pb collisions we find indications (see below) that the canonical freeze-out temperature, $T_f \approx 140$ MeV, might be too high for this larger system. Therefore we calculated the lead-on-lead collision also with freeze-out at $\varepsilon_f = 0.069$ GeV/fm^3 corresponding to an average freeze-out temperature of $T_f \approx 120$ MeV.

3.1 Spectra

Particle spectra are calculated using the prescription of Cooper and Frye [10] including the same hadrons as in the construction of the equation of state [4]. In the discussion

Fig. 3a–c. Initial density distributions for S+S (solid inner line), O+Au (dotted), S+Ag (dot-dashed), S+Au (dashed) and Pb+Pb (solid outer line) collisions. In panel **a** the baryon density n_B and in **b** the energy density ε are shown as functions of z on the symmetry axis $\rho = 0$. In panel **c** the radial dependence of energy density ε is shown at $z = 0$

drodynamical treatment of nucleus-nucleus collisions more realistic.

We show in Fig. 3 the initial local baryon density n_B and the local energy density $\varepsilon(z, \rho)$ for the five collisions we consider. In Fig. 3a $n_B(z, \rho)$ is plotted as function of z for $\rho = 0$. In all cases the stopping leads to approximately Gaussian distribution with the maximum at the global center-of-mass position for symmetric cases and slightly shifted towards the heavier target side for the asymmetric cases.
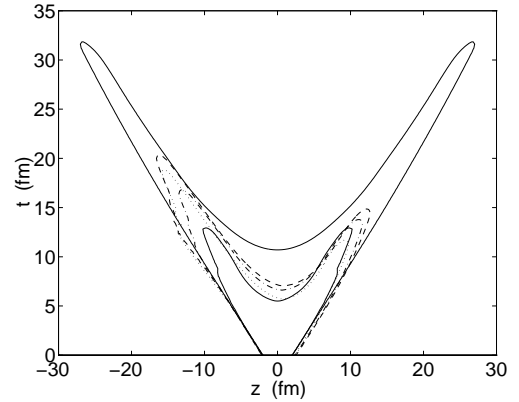
Table 1. Summary of parameters characterizing different nuclear collisions. A QGP equation of state with $T_c = 165$ MeV (EOS A [4]) is used. Quantities in the first part characterize the colliding system, those in the second part the initial conditions of produced matter where values of ξ and τ_0^{eff} are obtained from a fit to each specific collision, and the quantities in the third part describe the system at the freeze-out. For Pb+Pb collisions the numbers in parenthesis correspond to a freeze-out energy density $\varepsilon_f = 0.069$ GeV/fm^3 with an average freeze-out temperature of 120 MeV. The Bjorken estimates ε_{Bj} are deduced from experimental $dE_T/d\eta$ distributions taken from [32] and [33]

collision	S + S	O + Au	S + Ag	S + Au	Pb + Pb
$B + A$	32 + 32	16 + 197	32 + 108	32 + 197	207 + 207
lab. energy (GeV/A)	200	200	200	200	158
y_{cms}	3.03	2.54	2.73	2.62	2.92
ξ	0.9	1.0	0.9	0.95	0.9
τ_0^{eff} (fm/c)	1.2	1.4	1.4	1.5	1.3
$\overline{\varepsilon}_R$ (GeV/fm^3)	2.5	4.1	3.8	4.8	6.7
exp. ε_{Bj} (GeV/fm^3)	1.3	2.3	2.1	2.6	3.0
$\overline{T}_R(z=0)$ (MeV)	187	203	202	212	227
$R(\xi A)$ (fm)	3.15	6.37	4.96	6.37	6.25
$R(\xi B)$ (fm)	3.15	2.48	3.15	3.28	6.25
cent. t_f (fm/c)	6.3	6.5	7.5	8.0	11.8 (14.7)
$\langle v_\rho \rangle(|y_z| < 0.25)$ (c)	0.27	0.34	0.31	0.35	0.33 (0.44)

of particle spectra we concentrate on the most abundant particles, i.e. negative particles, pions and (net) protons because for them the hydrodynamical treatment with assumed chemical equilibrium is most reliable. We show in Fig. 5 the rapidity distributions of negative particles for the various collisions. A good agreement is seen in these rapidity spectra. To a small extent the agreement in the normalization is improved by adjusting the ξ parameter in (1) which accounts for the impact averaging. This parameter is determined for each collision system separately by optimizing the fit to the negative particles, but as shown in Table 1 the variations of ξ are quite small. The calculation for Pb+Pb collisions with the lower freeze-out temperature of 120 MeV is shown as dotted line in Figs. 5–8.

The rapidity spectra of negative particles are most sensitive to the initial energy distribution. Our parametrization (7) which includes only two free parameters c_ε and α_ε in the expression of the width (8) reproduces all five measured rapidity spectra of negative particles. This suggests that (7) could be used for any collision system at SPS energies. One should keep in mind, however, that the optimal values for the parameters c_ε and α_ε in (8) depend on the equation of state used for the hydrodynamical evolution.

The rapidity spectra of net protons are given in Fig. 6. For S+S the $p - \bar{p}$ distribution shows two maxima in the target and projectile fragmentation region which are nicely reproduced by the calculation. For Pb+Pb collisions stronger stopping is expected. The choice of parameters in (6) together with the EOS is able to account for the larger stopping in a quantitatively satisfactory way as seen from the comparison with preliminary data from NA49 [3].

In the asymmetric collisions the net proton rapidity distributions are reproduced only around midrapidity and in the forward region while at target fragmentation region the net proton yields are underestimated considerably. The reason for this deviation can be understood by considering the geometry of an asymmetric collision. The initial state of the hydrodynamical calculation is determined by using the cylindrical volume as cut out of the target by the smaller projectile nucleus. However, during the first collisions the projectile nucleons moving through the target acquire transverse momentum, some of them penetrate into the region outside the cylinder and interact further. Similarly some of the produced particles can interact with the nucleons outside the cylinder. Nucleons from these interactions are not included in the hydrodynamic description but are observed experimentally in the target fragmentation region. It is reasonable to assume that these additional protons will not play any role in the hydrodynamical calculation. This assumption is supported by the Λ rapidity distributions in Fig. 6 which show good agreement between the calculated and measured spectra even in the target fragmentation region.

In Fig. 7 we show that the measured transverse momentum distributions of negatives and π^0's agree quite well with the calculated spectra except in the case of O+Au collisions, where the large low-p_T enhancement cannot be reproduced and the calculation exhibits slightly too much flow. For Pb+Pb the very forward pions are flatter than in the calculation. The particle density at this edge of the phase space, however, is becoming so small that hydrodynamics with relatively strong longitudinal flow can lead to an artificially large transverse cooling. Thus we
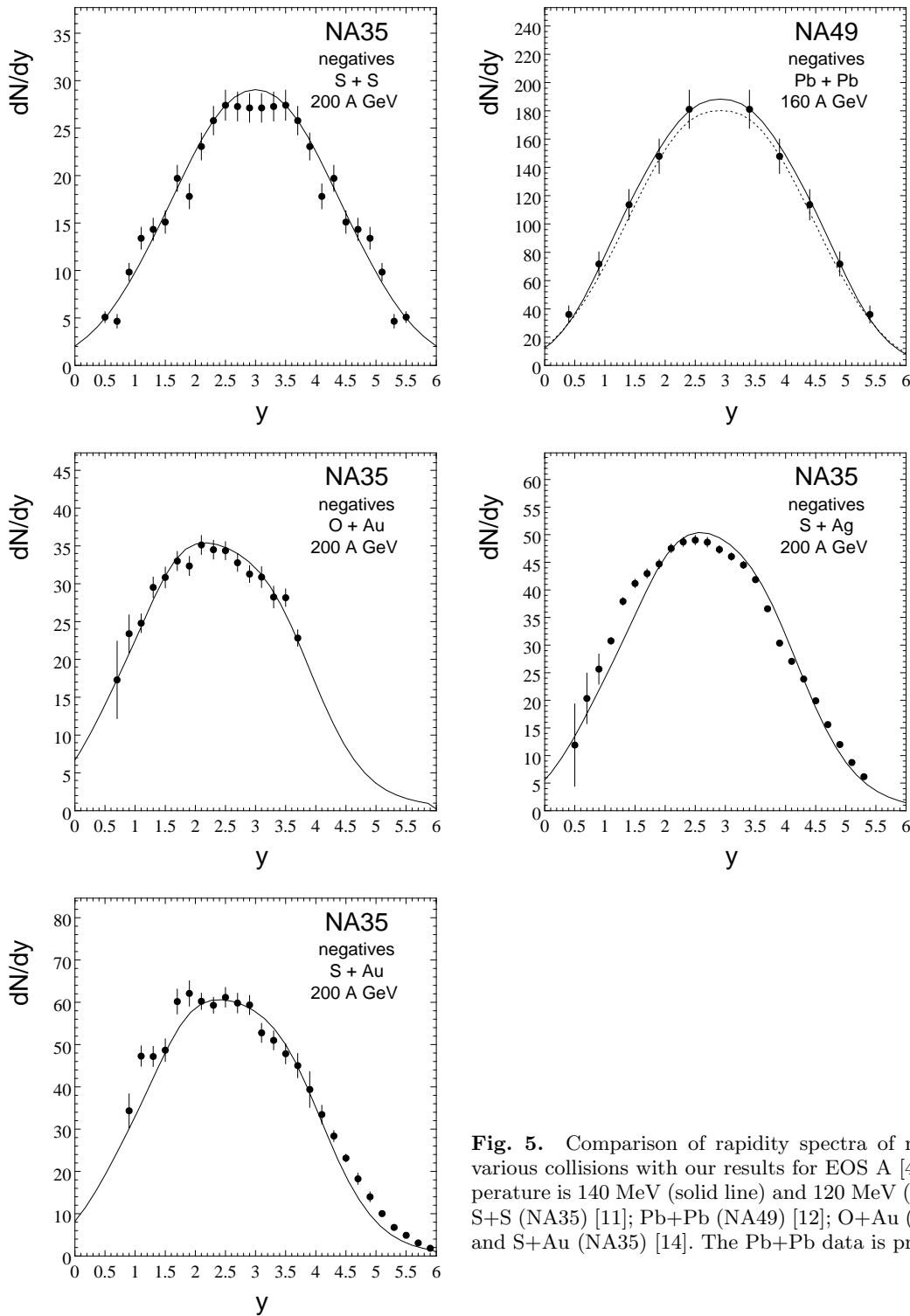
Fig. 5. Comparison of rapidity spectra of negative particles measured in various collisions with our results for EOS A [4]. The average freeze-out temperature is 140 MeV (solid line) and 120 MeV (dotted line). The data sets are: S+S (NA35) [11]; Pb+Pb (NA49) [12]; O+Au (NA35) [13]; S+Ag (NA35) [14] and S+Au (NA35) [14]. The Pb+Pb data is preliminary

should not expect that hydrodynamics can describe the far edges of fragmentation regions well.

A closer look on the experimental transverse spectra shows that nearly all of them have a small but visible concave shape in $m_T - m_0$ which is not reproduced by the calculation. The calculation gives only the average slope right. We think that the explanation is the too simple freeze-out procedure applied in the calculation. In fact, in such a small system as created in the nuclear collisions, the last interaction of a final hadron can take place with non-zero probability at any space-time point. Therefore the spectra receive contributions from all temperatures and not only from the assumed freeze-out temperature. Note that the number of particles in the tail of transverse distribution is very small indicating that rare earlier escapes of high–p_T particles would not invalidate the hydrodynamic
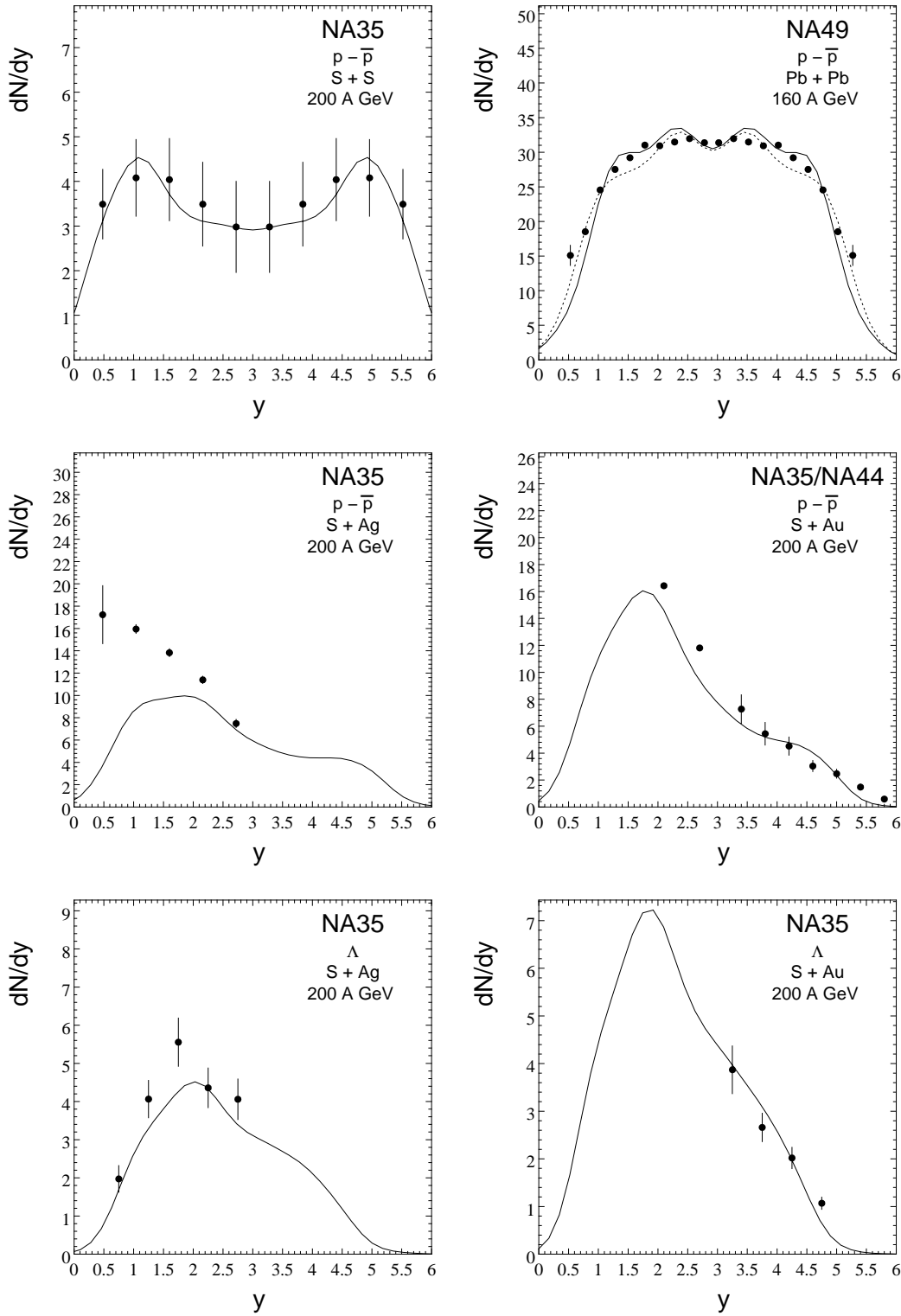
Fig. 6. Comparison of rapidity spectra of $p - \bar{p}$ and Λ measured in various collisions with our results for EOS A [4]. The average freeze-out temperature is 140 MeV (*solid line*) and 120 MeV (*dotted line*). The data sets are: $p - \bar{p}$ in S+S (NA35) [11]; $p - \bar{p}$ in Pb+Pb (NA49) [3]; $p - \bar{p}$ in S+Ag (NA35) [15]; $p - \bar{p}$ in S+Au (NA35: $y > 3$) [15] (two data points with $y < 3$ are proton data from NA44 [16]); Λ in S+Ag (NA35) [17] and Λ in S+Au (NA35) [17]. The Pb+Pb data is preliminary.
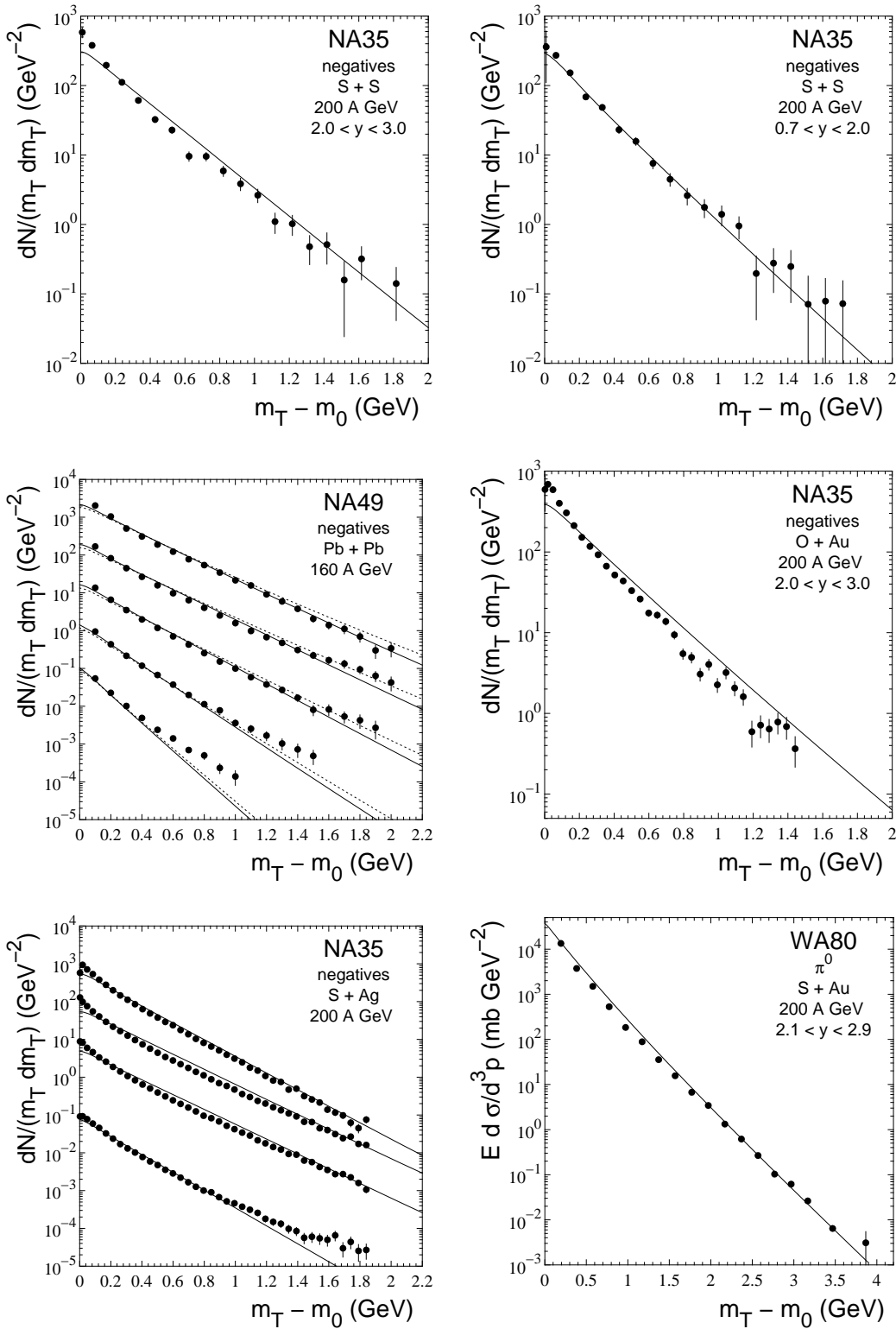
Fig. 7. Comparison of transverse momentum spectra of negative particles and π^0 measured in various collisions with our results for EOS A [4]. The average freeze-out temperature is 140 MeV (*solid line*) and 120 MeV (*dotted line*). The data sets are: S+S (NA35) [11]; Pb+Pb (NA49) [12] for rapidity intervals of width 0.5 and center at (top to bottom) 3.4, 3.9, 4.4, 4.9, 5.4 and data sets successively scaled down by 10^{-n}; O+Au (NA35) [13]; S+Ag (NA35) [15] for rapidity intervals (top to bottom) $0.8 \le y \le 2.0$, $2.0 \le y \le 3.0$, $3.0 \le y \le 4.0$, and $4.0 \le y \le 4.4$ and data sets successively scaled by 10^{-n} ($n = 0,1,2,3$); S+Au (WA80) [18]. The Pb+Pb data is preliminary
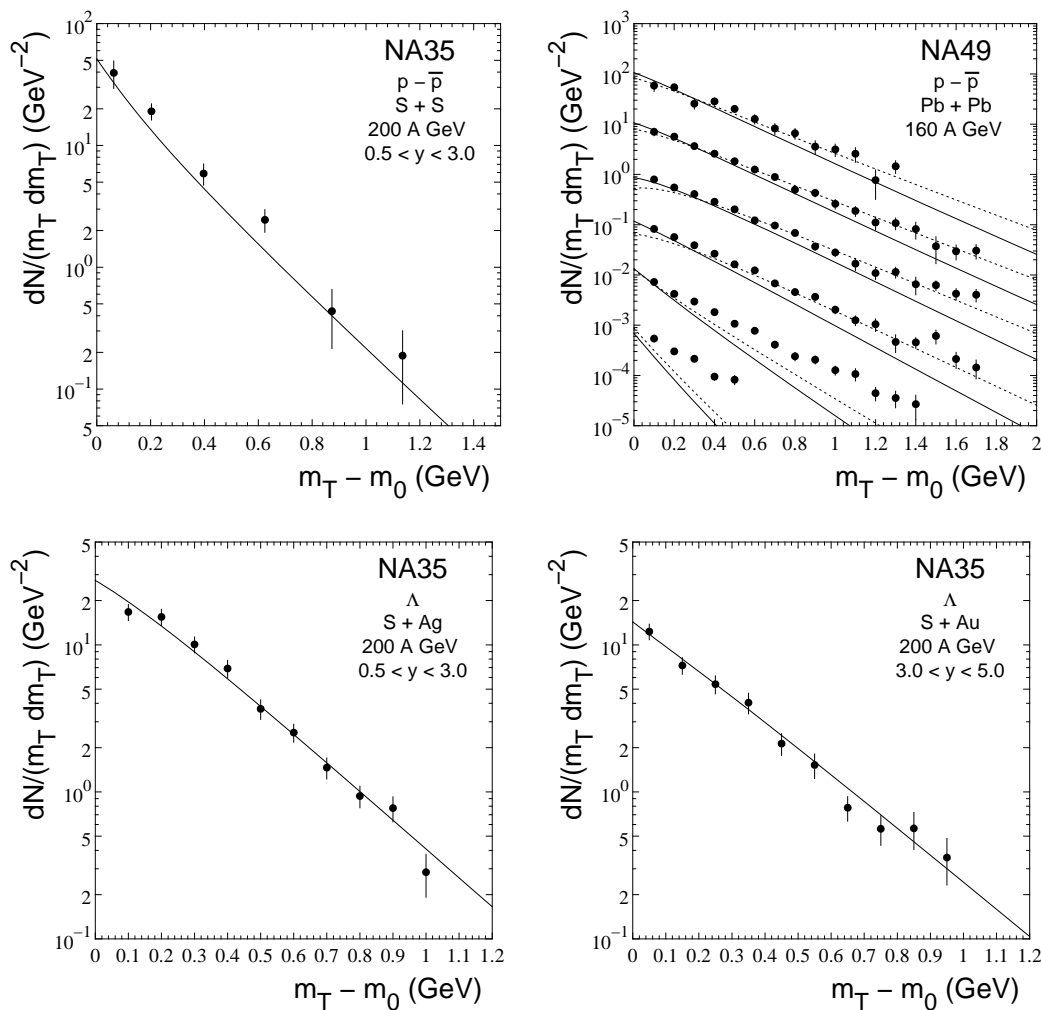
Fig. 8. Comparison of transverse momentum spectra of $p - \bar{p}$ and Λ measured in various collisions with our results for EOS A [4]. The average freeze-out temperature is 140 MeV (*solid line*) and 120 MeV (*dotted line*). The data sets are: $p - \bar{p}$ in S+S (NA35) [11]; $p - \bar{p}$ in Pb+Pb (NA49) [12] for rapidity intervals of width 0.5 and center at (top to bottom) 2.9, 3.4, 3.9, 4.4, 4.9, 5.4 and data sets successively scaled down by 10^{-n}; Λ in S+Ag (NA35) [17] and Λ in S+Au (NA35) [17]. The Pb+Pb data is preliminary

treatment of the bulk of the final matter. Improvements have been suggested [19] but they are difficult to implement technically.

Finally, we show in Fig. 8 the transverse momentum distribution of heavy particles. In S+S collisions the net proton distribution is in agreement with the data supporting the assumption of freeze-out at a common transverse flow velocity with pions. For S+Ag and S+Au we obtain agreement in the p_T-spectra of Λ's. The agreement in the normalization should be considered accidental. It is obtained with a freeze-out temperature of $T_f \approx 140$ MeV and assuming full chemical equilibration. More detailed studies on chemical equilibration indicate higher chemical freeze-out temperatures but not full chemical equilibration of strangeness [20,21]. In our calculation the normalization is achieved because the lower freeze-out temperature is compensated by the assumption of full chemical equilibration of Λ's. In the transverse spectrum the lower freeze-out temperature is balanced by the transverse flow.

For Pb+Pb collisions the calculated transverse spectrum of net protons is slightly steeper than the data even at central rapidities if a freeze-out temperature $T_f \approx 140$ MeV is used. This was already observed in [22] and is an indication of the freeze-out taking place at lower temperature in the larger Pb+Pb system. Therefore we redid the calculation with a freeze-out temperature $T_f \approx 120$ MeV as suggested in [23–25]. The result is shown as dotted line in Fig. 8. The agreement for the transverse spectrum of net protons is clearly improved. The corresponding m_T-spectrum of negatives in Fig. 7 is only slightly modified compared to the freeze-out at $T \approx 140$ MeV.

We did a calculation for S+S collisions with $T_f = 120$ MeV, too. While the p_T slope of negatives still agrees with the data, that of net-protons, and in particular that of kaons and lambdas, comes out flatter than the data.

We conclude that our calculations support the kinetic estimates for the freeze-out [9], especially its dependence on the size of the system. However, the freeze-out tem-

peratures favoured by the p_T-spectra are model dependent since we found that results for Pb+Pb collisions with $T_c = 200$ MeV and $T_f \approx 140$ MeV are close to those with $T_c = 165$ MeV and $T_f \approx 120$ MeV.

3.2 Parameter systematics

We next discuss the A-dependence of various quantities in our model. In Table 1 we show parameters which define the collision (upper part) and describe the initial and freeze-out state. The parameters ξ and τ_0^{eff} have been adjusted to each collision system. ξ is always close to one showing that the experiments were triggered to most central collisions and include nearly the whole energy and baryon number. The symmetric collisions show a trend to a lower value of ξ indicating that the impact averaging is more important for these cases.

The τ_0^{eff} determines the slope of the initial rapidity profile (10) as function of z and thus the spatial distributions of densities. A simultaneous fit to the longitudinal and transverse spectra determines the optimal τ_0^{eff}. It turns out that τ_0^{eff} is very similar, $\tau_0^{\mathrm{eff}} \sim 1.3$ fm/c, for all collisions from S+S to Pb+Pb. However, the sensitivity of final spectra on τ_0^{eff} is not very strong, since the density parametrizations are done in rapidity space. Within a variation of ± 0.2 fm/c in τ_0^{eff} the fits remain acceptable.

As mentioned already earlier, τ_0^{eff} can be considered to give an estimate of the thermalization time. On the other hand the initial longitudinal extension can be related to the equilibration time for the whole system in the global center-of-mass frame. The longitudinal extension of all systems is roughly the same and leads to an estimate of a common initial time of around 3 fm/c as counted from the time when the front edges of the nuclei meet to the time when all quanta from primary collisions have formed and reached approximate equilibrium. The difference compared to τ_0^{eff} arises mainly from the finite thickness of colliding nuclei. The numbers are consistent with the findings in the three-fluid hydrodynamical studies. They indicate a pressure equilibration time to be of the order of 1.5 fm/c for Pb+Pb collisions [26] at SPS energies. In the hydrodynamic treatment, carried out in the center-of-mass system of participating nuclei, the initial conditions are specified at global equilibration time of the whole system which, however, does not enter the calculation as an explicit parameter.

In Table 1 we give values of the energy density ε of the initial fireball formed in different collisions. We average over the transverse area in a unit rapidity interval at $y = 0$,

$$\bar{\varepsilon}_R = \frac{\int d\rho\,\rho\,\varepsilon(\rho)}{\int d\rho\,\rho}, \qquad (13)$$

in order to compare with various estimates, in particular with those from the experimental transverse energy flow.

We expect the A-dependence of the initial energy density to lie between the following two crude estimates based on the assumption that ε is proportional to the number of sources in a nucleus-nucleus collision. An upper limit is
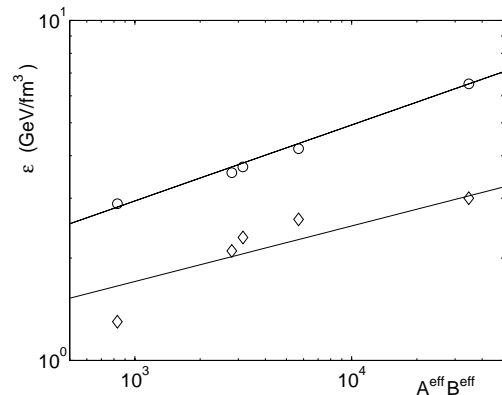

Fig. 9. Initial average energy density plotted against $A^{\mathrm{eff}}B^{\mathrm{eff}}$. Open circles show the calculated values (13) and the diamonds the Bjorken estimates (17) from experimental data [32, 33] with lines corresponding to minimum χ^2 fits of the form (16)

provided by the possibility that each nucleon in the projectile can interact with any nucleon on its path through the target and v.v. with probabilities given, e.g. by the Glauber model [27]. The assumption that the energy of the nucleons is degraded independently in each collision with a certain fraction transferred to the fireball, leads to the scaling of the energy density as

$$\varepsilon^{\mathrm{Gl}} \propto T_A\,T_B \propto R_A\,R_B \propto (AB)^{1/3}. \qquad (14)$$

The other extreme is the wounded nucleon model [28] which assumes that each nucleon contributes as a single source, see also [8]. Then the number of sources on the symmetry axis is proportional to $T_A + T_B$ with a scaling behaviour, which for the mass numbers of interest, can be approximated with the form

$$\begin{aligned}
\varepsilon^{\mathrm{WN}} &\propto T_A + T_B \propto R_A + R_B \\
&\propto A^{1/3} + B^{1/3} = (AB)^{1/6}\left[(A/B)^{1/6} + (B/A)^{1/6}\right] \\
&\approx 2(AB)^{1/6}.
\end{aligned} \qquad (15)$$

It should be kept in mind that the physics of particle production is expected to depend on the collision energy. Soft processes can dominate at the SPS energy but at RHIC and in particular at LHC the hard and semi-hard production of jets and minijets will probably be the main mechanism [29, 30]. This means that the mass number scaling of ε will be different at different energies.

We investigate the scaling behaviour of the initial energy density by fitting the A-dependence with

$$\varepsilon = \varepsilon_0\,(A^{\mathrm{eff}}B^{\mathrm{eff}})^\gamma. \qquad (16)$$

The fit to the transversely averaged calculated values $\bar{\varepsilon}_R$ (open circles) against the product of effective mass numbers $A^{\mathrm{eff}}B^{\mathrm{eff}}$ (cf. (1)) is shown in a double logarithmic plot in Fig. 9. The minimum χ^2-fit to the five collision systems results in $\gamma = 0.22$.

The result is between the two examples mentioned above (cf. (14) and (15)), somewhat closer to the wounded

nucleon alternative than the Glauber type behaviour. The classical Glauber treatment (14) neglects possible interference effects like the Landau–Pomeranchuck–Midgal effect [31] which could lead to a weaker dependence on the mass numbers. On the other hand, in the wounded nucleon picture the effects of multiple interactions may require an increase of the source strength per nucleon leading to faster growth than the approximate $(AB)^{1/6}$ behaviour.

Our initial energy density may also be compared with the estimates from the experimental transverse energy flow (or multiplicity densities) using the Bjorken model for the initial volume [8]:

$$\varepsilon_{\mathrm{Bj}} = \frac{(\mathrm{d}E_T/\mathrm{d}\eta)_{\max}}{\pi R_{\mathrm{proj}}^2 \tau_0} \ . \tag{17}$$

These results for $\tau_0 = 1$ fm/c, taken from [32] and [33], are also shown in Fig. 9 together with the fit, (16). The χ^2-fits for the $\bar{\varepsilon}_R$ values in our model and the Bjorken estimates from experiment are:

$$\bar{\varepsilon}_R = 0.63 \,\mathrm{GeV/fm}^3 \ \left(A^{\mathrm{eff}} B^{\mathrm{eff}}\right)^{0.22} \tag{18}$$

$$\varepsilon_{\mathrm{Bj}} = 0.55 \,\mathrm{GeV/fm}^3 \ \left(A^{\mathrm{eff}} B^{\mathrm{eff}}\right)^{0.16} \ . \tag{19}$$

It is interesting to notice that $\varepsilon_{\mathrm{Bj}}$ has the scaling of $(AB)^{1/6}$ as expected from the wounded nucleon picture.

We see in Fig. 9 that our average initial energy density is roughly a factor of two higher than the Bjorken estimate. This difference reflects the assumed hydrodynamic behaviour. In the hydrodynamic expansion the thermal energy is transferred to collective flow motion by the expansion work of pressure. When the flow is asymmetric in longitudinal and transverse directions the stronger longitudinal flow leads to larger energy transfer into the longitudinal degrees of freedom. As a result the energy per unit rapidity is decreased in the central rapidity region and increased in the fragmentation regions. If we calculate the initial energy density using the Bjorken estimate, (17) from our calculated final spectra, we obtain numbers which are consistent with the estimates from experiment.

We would like to point out that the scaling of energy density is not very sensitive to the parameters used in (2) for the initial baryon distributions. The initial energy density is dominantly given by the τ_0^{eff} and the parametrization of the width σ_ε (8) in the Gaussian energy distribution (7). This parametrization is fitted to the rapidity spectra of negative particles. Therefore the scaling in the initial energy density is mainly extracted from the experimental pion spectra.

We next discuss quantities which characterize the freeze-out. The lifetime t_f of the fireball, defined as the freeze-out time at the center, increases as expected with the size of the fireball. We see a doubling of the lifetime when going from S+S to Pb+Pb indicating approximately linear dependence on the nuclear radius.

An important quantity from the point of view of the hadron spectra is the transverse flow velocity at freeze-out. In a local hydrodynamical calculation the transverse flow is different for different fluid cells. In order to compare

with average flow velocities of simpler models [34] or phenomenologically extracted values [35] we have to average over the relevant range of the freeze-out surface. At central rapidities we choose for convenience to average over all fluid cells with rapidity $|y| < 0.25$ in the global fireball rest frame. This corresponds to the region of highest transverse flow. The resulting values for $\langle v_\rho \rangle$ are given in Table 1. Note that the range $|y| < 0.25$ does not necessarily correspond to the rapidity region where the transverse momentum spectra in Figs. 7 and 8 are measured.

The numbers for $\langle v_\rho \rangle$ are very similar with the exception of S+S. The fact that we get for O+Au a rather similar average flow velocity than for Pb+Pb is a result of taking the same freeze-out energy density independent of collision size. Using for Pb+Pb collisions the lower freeze-out energy density corresponding to $T_f \approx 120$ MeV we find a considerable stronger flow than in the smaller systems. A system-size dependent freeze-out can naturally be incorporated if one uses a dynamical freeze-out criteria as suggested in [34,24] resulting in a decrease of freeze-out temperature with increasing nuclear size.

The flow values for the symmetric collisions may be compared with the data analysis of NA44 [35]. They extracted the mean transverse velocity from a fit to various hadron spectra obtaining $\langle v_\rho \rangle = 0.24 \pm 0.10$ for S+S and $\langle v_\rho \rangle = 0.36 \pm 0.14$ for Pb+Pb [35] in agreement with our studies. Our freeze-out temperature $T_f \approx 140$ MeV agrees with their fitted value $T_f = 142 \pm 5$ MeV for S+S. But for Pb+Pb they favour a somewhat higher value $T_f = 167 \pm 13$ MeV while our results favour the lower freeze-out temperature of 120 MeV leading to $\langle v_\rho \rangle = 0.44$ for Pb+Pb in agreement with [23].

4 Conclusions

We have constructed a model for initial conditions in nucleus-nucleus collisions at CERN-SPS energies based on the parametrization of baryon stopping by specifying the initial baryon number distribution dN_{B}/dy. The parametrization is expressed as a function of the local thickness of colliding nuclei in the transverse plane. The major advantages of this approach are that it reduces the arbitrariness of choosing the initial conditions for different collisions and allows a proper treatment of transverse geometry of the colliding nuclei. We think that this is an important improvement compared to the earlier approaches [4,5] where different collisions are not related and the longitudinal dependence is treated equally both on the symmetry axis at $\rho = 0$ and at the outer edge ($\rho = R_{\mathrm{P}}$) of the collision system.

The success in reproducing the single particle spectra for various collisions gives confidence that the deduced mass number dependencies of the initial and final state quantities are reasonable. An important example is the scaling of the the initial energy density. Even though the observed dependence of hadron multiplicity on the mass number is close to linear, corresponding to the $(AB)^{(1/6)}$ scaling for the density, the initial energy density grows

faster as shown in Fig. 9 reflecting the effect of hydro-dynamic expansion on the final transverse energy flow. For the S+Au and Pb+Pb collisions we obtain a ratio $\varepsilon_{S+Au}/\varepsilon_{Pb+Pb} \approx 2/3$ which, in addition to the volume effects, could be related to the observed features of J/Ψ suppression [36]. In our parametrization the center of the fireball starts out in the quark-gluon plasma phase for all considered collisions. However, we consider the scaling more reliable than the absolute value of energy density which is more sensitive on the details of the parametrization. One should also note that in smaller systems the high density occurs only for a short time interval in a small fraction of the total volume.

For further improvements in determining the initial conditions of nuclear collisions a better understanding of the freeze-out physics is needed, e.g. to allow emission from the whole space–time volume [19]. For a proper treatment also a sequential freeze-out for various particle species should be implemented [24]. Since the particle ratios are a result of the whole evolution and not only of the freeze-out conditions this would help more directly in pinning down the initial state in nuclear collisions.

References

1. H. Satz, Proceedings of the *Int. Conference on the Physics and Astrophysics of the Quark-Gluon Plasma*, (Jaipur/India March 1997) edited by B.C. Sinha, D.K. Srivastava, Y.P. Viyogi, in press (University of Bielefeld preprint BI-TP 97/22;hep-ph/9706342)
2. Proceedings of the *Int. Workshop on Applicability of Relativistic Hydrodynamical Models in Heavy Ion Physics*, edited by D. Strottman, L. Csernai, B. Müller, Heavy Ion Physics **5** (1997)
3. P. Jacobs et al. (NA49 collaboration), Proceedings of the *Int. Conference on the Physics and Astrophysics of the Quark-Gluon Plasma*, (Jaipur/India March 1997) edited by B.C. Sinha, D.K. Srivastava, Y.P. Viyogi, in press
4. J. Sollfrank, P. Huovinen, M. Kataja, P.V. Ruuskanen, M. Prakash, R. Venugopalan, Phys. Rev. C **55**, 392 (1997)
5. U. Ornik, R.M. Weiner Phys. Lett. **263B**, 503 (1991); B.R. Schlei, U. Ornik, M. Plümer, D. Strottman, R.M. Weiner Phys. Lett. **376B**, 212 (1996); U. Ornik, M. Plümer, B.R. Schlei, D. Strottman, R.M. Weiner, Phys. Rev. C **54**, 1381 (1996)
6. J. Sollfrank, P. Huovinen, P.V. Ruuskanen, Heavy Ion Physics **5**, 321 (1997)
7. A. Bohr, B.R. Mottelson, *Nuclear Structure*, Vol. 1, (W.A. Benjamin,Inc, New York, 1969)
8. J.D. Bjørken, Phys. Rev. D **27**, 140 (1983)
9. J.L. Goity, H. Leutwyler, Phys. Lett. **228B**, 517 (1989); M. Prakash, M. Prakash, R. Venugopalan, G. Welke, Phys. Rep. **227**, 323 (1993); E. Schnedermann, U. Heinz, Phys.

10. F. Cooper, G. Frye, Phys. Rev. D **10**, 186 (1974)
11. J. Bächler et al. (NA35 collaboration), Phys. Rev. Lett. **72**, 1419 (1994)
12. P.G. Jones et al. (NA49 collaboration), Nucl. Phys. **A610**, 188c (1996)
13. T. Alber et al., (NA35 collaboration), Eur. Phys. J. **C2**, 643 (1998)
14. M. Gaździcki et al. (NA35 collaboration), Nucl. Phys. **A590**, 197c (1995)
15. D. Röhrich et al. (NA35 collaboration), Nucl. Phys. **A566**, 35c (1994)
16. M. Murray et al. (NA44 collaboration), in *Strangeness '95*, AIP Conference Proceedings **340**, edited by J. Rafelski, (AIP Press, 1995), p. 162
17. T. Alber et al. (NA35 collaboration), Z. Phys. C **64**, 195 (1994)
18. R. Santo et al. (WA80 collaboration), Nucl. Phys. **A566**, 61c (1994)
19. F. Grassi, Y. Hama, T. Kodama, Phys. Lett. **355B**, 9 (1995)
20. J. Sollfrank, J. Phys. G **23**, 1903 (1997)
21. F. Becattini, M. Gaździcki, J. Sollfrank, Eur. Phys. J. **C5**, 143 (1998)
22. B. Schlei, Heavy Ion Physics **5**, 403 (1997); B. Schlei, D. Strottman, N. Xu, Phys. Rev. Lett. **80**, 3467 (1998)
23. B. Kämpfer, preprint FZR-149 (hep-ph/9612336)
24. C.M. Hung, E. Shuryak, Phys. Rev. C **57**, 1891 (1998)
25. U. Wiedemann, B. Tomášik, U. Heinz, Proccedings of QM'97, Nucl. Phys. **A** in press, (nucl-th/9801017)
26. A. Dumitru, J. Brachmann, M. Bleicher, J. Mahrun, H. Stöcker, W. Greiner, Heavy Ion Physics **5**, 357 (1997)
27. R.J. Glauber, in *Lectures in Theoretical Physics*, edited by W.E. Brittin, L.G. Dunham (Interscience, New York, 1959), Vol. 1, p. 315
28. A. Bialas, M. Bleszyńsky, W. Czyż, Nucl. Phys. **B111**, 461 (1976)
29. K.J. Eskola, K. Kajantie, J. Lindfors, Nucl. Phys. **B323**, 37 (1989); K.J. Eskola, K. Kajantie, P.V. Ruuskanen, Phys. Lett. **332B**, 191 (1994)
30. X.N. Wang, Phys. Rep. **280**, 287 (1997)
31. L.D. Landau, Dokl. Akad. Nauk. SSSR **92**, 535 and 735 (1953); A.B. Migdal, Phys. Rev. **103**, 1811 (1956)
32. J. Bächler et al. (NA35 collaboration), Z. Phys. C **52**, 239 (1991)
33. S. Margetis et al. (NA49 collaboration), Nucl. Phys. **A590**, 355c (1995)
34. E. Schnedermann, U. Heinz, Phys. Rev. C **47**, 1738 (1993); E. Schnedermann, J. Sollfrank, U. Heinz, Phys. Rev. C **48**, 2468 (1994); U. Mayer, U. Heinz, Phys. Rev. C **56**, 439 (1997)
35. I.G. Bearden et al. (NA44 collaboration), Phys. Rev. Lett. **78**, 2080 (1997)
36. M. Gonin et al. (NA50 collaboration), Nucl. Phys. **A610**, 404c (1996)
37. D. Kharzeev, C. Laurenzo, M. Nardi, H. Satz, Z. Phys. C **74**, 307 (1997); D. Kharzeev, Nucl. Phys. **A610**, 418c (1996)

Rev. C **50**, 1675 (1994); H. Sorge, Phys. Lett. **373B**, 16 (1996)